Numerical Analysis of the Perona-Malik Fractional Nonlinear Anisotropic Diffusion Problem for Image Noise Removal

Mardo Victor Gonzales Herrera,
Saulo Murillo and Miguel Dumett

November 25, 2025

Publication Number: CSRCR2025-06

Computational Science & Engineering Faculty and Students Research Articles

Database Powered by the Computational Science Research Center Computing Group & Visualization Lab

COMPUTATIONAL SCIENCE & ENGINEERING

SAN DIEGO STATE UNIVERSITY

Computational Science Research Center
College of Sciences
5500 Campanile Drive
San Diego, CA 92182-1245
(619) 594-3430

NUMERICAL ANALYSIS OF THE PERONA-MALIK FRACTIONAL NONLINEAR ANISOTROPIC DIFFUSION PROBLEM FOR IMAGE NOISE REMOVAL

MARDO VICTOR GONZALES HERRERA, SAULO MURILLO AND MIGUEL DUMETT

Abstract. This work numerically solves the fractional-time nonlinear diffusion equation with Neumann-type boundary conditions, modeled by the Perona-Malik equation, which is used for image processing. The numerical scheme employs forward finite differences to discretize the time variable and mimetic differences to discretize spatial variables. The fractional extension introduces a memory effect that assists in image smoothing without erasing edges. Different numerical methods are analyzed and compared for both, the integer and the fractional cases; however, the proposed numerical scheme proves to be highly efficient when considering practical experiments in processing various images. Furthermore, the proposed model exhibits good visual quality performance as measured by metrics such as signal-to-noise ratio (SNR) and peak-to-noise ratio (PSNR).

Keywords: Nonlinear anisotropic diffusion Equation, MOLE, Mimetic Operators, Mimetic Discretization.

Contents

1. Introduction and main results

During the last decade, there has been widespread interest in solving various applications related to the analysis and processing of images described by the nonlinear anisotropic diffusion equation and its ability to eliminate noise in medical and scientific images, which present critical situations such as textures, edges, and contours.

The usage of integer-order in the nonlinear anisotropic diffusion equation for image noise removal introduces unwanted terms such as the stair-step effect and the speckle effect, both of which alter or distort the original image. Thus, in 2012, Hu et al. [3] proposed a new scheme called fractional-order nonlinear anisotropic diffusion, which replaces the integer-order derivative in the Perona-Malik nonlinear diffusion model with the fractional derivative of Grunwald Letnikov (L-G). This provides a more flexible way to remove noise from images while preserving the most relevant anatomical details. The results show that this technique, with appropriate diffusion parameters, effectively suppresses the stair-step and speckle effects. Furthermore, fractional-order Perona-Malik diffusion also exhibits good performance in terms of visual quality and mean square error calculations.

The Perona-Malik anisotropic diffusion technique is commonly used for image noise removal, proving highly useful and efficient if diffusion parameters are properly selected. However, incorrect parameter calculations can lead to over-smoothing or unfiltered noise. Therefore, selecting the diffusion parameters is crucial. In 2014, Abd et al. [5] numerically solved the Perona-Malik anisotropic diffusion model using a finite difference approach. The discretized model was evaluated using different exponential and quadratic diffusion coefficients on defective radiographic images. The model's performance was also verified using metrics such as peak signal-to-noise ratio (PSNR) and structural similarity measure (SSIM), demonstrating that the finite difference approach effectively improves image quality and efficiency by removing noise from defective radiographic images.

Then in 2021, Yu et al. [10] developed a new model for images with complex structure and texture information. The research focused on determining a new reconstruction and noise reduction model for fractional-order super-resolution images with adaptive fidelity, based on the fractional nonlinear diffusion equation. An adaptive gradient operator was then constructed to balance the smoothing of the diffusion equation, the gradient fidelity term, and the ability to retain edge information in the image. A filter was then introduced into the model as a control term to improve the stability of the proposed model. Finally, the original fractional diffusion model was improved, and the fractional order was adaptively modified based on the local variance of the image, which effectively reduces the ladder effect in the image reconstruction process. The simulation results show that the proposed model not only reduces the ladder effect in the reconstruction and noise reduction process of super-resolution images but also exhibits good noise reduction performance by effectively preserving image edge information.

Thus, in 2023, Maiseli [4] proposed a new method that integrates a kernel which properly guides the diffusion process in all regions of the image. Experimental results show that the construction of his kernel promotes effective noise removal; specifically, its implementation highlights the establishment of diffusion kernel tuning constants, preserving significant image features.

However, another image processing technique has emerged that is non-invasive, non-intrusive, radiation-free, and cost-effective for generating cross-sectional images: electrical capacitance tomography (ECT). Despite its advantages, the low quality of its reconstructed images limits its applicability. Thus, in 2024, Nyotoka et al [12] developed a new algorithm that integrates the ECT model with a modified Perona-Malik function, capable of eliminating diffusion-directed image noise. This improves the quality of ECT reconstructed images beyond existing traditional methods, and qualitative evaluations indicate that the proposed algorithm demonstrates substantial improvements in image reconstruction quality. The algorithm effectively addresses the challenges of nonlinearity and poor posture, generating superior image quality compared to traditional methods such as linear back projection (LBP) and Landweber projection (PLAND).

Due to the low quality of the images generated by electrical capacitance tomography, which are often used only for qualitative analysis, this limitation stems from a nonlinear relationship between the measured capacitances and the permittivity distribution, as well as from the poor configuration of the sensitivity matrix elements. This hinders the applicability of ECT in online industrial process monitoring. Then in 2024, Dismas et al. [14] proposed a new method for image reconstruction, based on a nonlinear diffusion function that generates high-quality images from measured capacitance data of the ECT system. The diffusion regularization function helps to eliminate noise and preserve semantic features. Experimental results reveal that the proposed method generates high-quality and visually appealing images, with a 15% reduction in distribution error and a 10% increase in the correlation coefficient, compared to state-of-the-art methods such as linear back-projection and Landweber projection. This allowed for a greater impact on research into how nonlinear anisotropic diffusion can improve the applicability of ECT systems in industrial control and monitoring.

In 2024, Carrillo and Dumett [13] used the Enhanced Mimetic Operator Library (MOLE) to construct discrete analogs of the discrete gradient and divergence operators given in [15], used to solve image processing situations of some techniques described by partial differential equations (PDEs) for blur correction. In this way, they used a fundamental image enhancement technique called the shock filter, and provided a brief overview of the computational and mathematical procedures involved in using this technique to sharpen edges and improve image clarity.

Then in 2022, Sayah et al. [11] numerically solved the fractional-time nonlinear anisotropic diffusion equation of Perona-Malik. This model is derived from the standard Perona-Malik equation by replacing the integer-order ordinary derivative with a fractional Caputo derivative with respect to the time variable. Its numerical solution is based on the forward finite difference method to discretize the time variable and the centered finite difference scheme for discretizing the space variable. They presented some experimental results obtained by applying the proposed model to images degenerated by Gaussian noise. This noise is common in images acquired with cameras and telescopes that distort all the image pixels. The mathematical model of fractional-time nonlinear anisotropic diffusion was compared with the standard Perona-Malik model and/or the classical heat equation.

They considered the number of iterations set at 17, and the performance of the models was evaluated using the PSNR and SNR (signal-to-noise ratio) metrics, observed that the SNR/SNR metrics obtained for the proposed model for different values of the fractional exponent and variance are superior to those of other integer-order models.

Recently, Corbino and Castillo [15] developed an Improved Mimetic Operator Library (MOLE), a high-quality, open-source virtual library that integrates algorithms written in software such as C++ and Matlab, and implements the high-order mimetic differences (MD) method to solve partial differential equations in one-dimensional (1D), two-dimensional (2D), and three-dimensional (3D) space environments, with relative ease. They also provided discrete analogues of the most common vector calculus operators, such as gradient, divergence, curl, and Laplacian. These discrete operators (matrices) act on alternating meshes (uniform, non-uniform, and curvilinear) that satisfy local and global conservation laws.

Motivated by the aforementioned research and the valuable information we can obtain from image edges, our interest lies in numerically solving the fractional-time nonlinear anisotropic Perona-Malik diffusion equation with Neumann boundary conditions, considering the results obtained in [11], [13], and [6]. To avoid image blurring and control diffusion near the edges, the Perona-Malik model uses a non-homogeneous diffusion coefficient that, under certain conditions, allows smoothing within each region while preventing information diffusion across the edges.

Following [11] ideas, the following problem is studied:

$$ {}_0^cD_t^\alpha u(x,y,t) = div\left(C\left(\|\nabla u\left(x,y,t\right)\|\right)\nabla u\left(x,y,t\right)\right) \quad in \;\; \Omega \times I \tag{1.1}$$

Neumann-type boundary

ecua2

$$ \frac{\partial u\left(x,y\right)}{\partial n} = 0 \;\; on \;\; \partial\Omega \times I \tag{1.2}$$

Initial condition (Function intensity of the original image)

$$ u(x,y,0) = u_0(x,y) \;\; on \;\; \; (x,y) \in \Omega \tag{1.3}$$

where

- $\Omega \subset \mathbb{R}^2$ denotes a rectangular domain of $\mathbb{R}^2$.
- ${}_0^cD_t^\alpha$ represents the fractional-order derivative at the time of order α and in the sense of Caputo with $0 < \alpha < 1$, such that:

$$ {}_0^cD_t^\alpha u(x,y) = \frac{1}{\Gamma\left(1-\alpha\right)}\int_0^t \frac{\partial u\left(x,y\right)}{\partial s}\frac{ds}{\left(t-s\right)^\alpha} \tag{1.4}$$

- $u\left(x,y,t\right)$ represents the intensity function of the smoothed image at the position $(x,y) \in \Omega$ in time $t \in I$.
- $u_0\left(x,y\right)$ denotes the intensity function of the original image.
- ∇ represents the gradient operator.
- $\nabla\cdot$ denotes the divergence operator.
- $\dfrac{\partial u}{\partial n}$ represents the exterior unit normal derivative at the boundary.
- $I = [0,T] \;\; , \;\; T > 0$.
- Γ denotes the gamma function.
- $C : \mathbb{R}_0^+ \to \mathbb{R}^+$ represents the decreasing diffusion function.
- $u : \Omega \times I \to R$ is an infinitely differentiable function that represents the image intensity.

The model proposed by Perona and Malik given in [6], provides two diffusion coefficients expressed as:

$$C\left(|\nabla u|\right) = e^{\left(-\left(\frac{|\nabla u|}{K}\right)^2\right)} \tag{1.5}$$

and

$$C\left(|\nabla u|\right) = \frac{1}{\left(1+\left(\frac{|\nabla u|}{K}\right)^2\right)} \tag{1.6}$$

where K is a positive constant capable of controlling the sensitivity at the image edges. Here it is set manually; the methodologies for estimating the contrast parameter are presented in [7] [8] or depending on the noise in the image.

Thus, the main objective of the anisotropic model is fundamentally to incorporate a function that prevents smoothing at the edges of the image, called the diffusion function.

If the diffusion coefficient were made constant at all positions, smoothing would proceed isotropically; however, if smoothing varies according to the behavior of the local gradient of the image, anisotropic diffusion occurs.

2. Proposed Numerical Method

Discretization in the Time Variable. For this case, we will use the explicit finite difference scheme to discretize the time variable. Following the ideas of [2] we have:

The time interval $[0, T]$ is then partitioned into sub-intervals as follows.

Let $\mathbf{x} = (x, y) \in \Omega \subset \mathbb{R}^2$, and $0 = t_0 < t_1 < t_2 \cdots < t_n = T$ with step size $\triangle t = T/n$, where $t_k = k\triangle t$, $k = 0, 1, 2, \cdots, n-1, n$.

$$\frac{\partial^\alpha u(\mathbf{x}, t_{k+1})}{\partial t^\alpha} = \frac{1}{\Gamma(1-\alpha)} \sum_{j=0}^{k} \int_{t_j}^{t_{j+1}} \frac{\partial u(\mathbf{x}, s)}{\partial s} \frac{ds}{(t_{k+1}-s)^\alpha} \tag{2.1}$$

ecua7

$$\frac{\partial^\alpha u(\mathbf{x}, t_{k+1})}{\partial t^\alpha} = \frac{1}{\Gamma(1-\alpha)} \sum_{j=0}^{k} \frac{u(\mathbf{x}, t_{j+1}) - u(\mathbf{x}, t_j)}{\Delta t} \int_{t_j}^{t_{j+1}} \frac{ds}{(t_{k+1}-s)^\alpha} + r_{\Delta t}^{k+1} \tag{2.2}$$

where:

$$r_{\Delta t}^{k+1} \leq c_u \left[\frac{1}{\Gamma\left(1-\alpha\right)} \sum_{j=0}^{k} \int_{t_j}^{t_{j+1}} \frac{t_{j+1} + t_j - 2s}{(t_{k+1}-s)} ds + O\left(\Delta t^2\right) \right], \tag{2.3}$$

is the truncation error given in [2] and c_u is a positive constant that depends only on u

$$r_{\Delta t}^{k+1} \leq c_u . 2\Delta t^{2-\alpha}. \tag{2.4}$$

Then, after performing the calculations corresponding to the integral given in (2.2), it is obtained:

$$\begin{aligned}\frac{\partial^{\alpha}u(\mathbf{x},t_{k+1})}{\partial t^{\alpha}} &= O\left(\alpha,\Delta t\right)\sum_{j=0}^{k}\left(u\left(\mathbf{x},t_{k-j+1}\right)-u\left(\mathbf{x},t_{k-j}\right)\right)\left[(j+1)^{1-\alpha}-(j)^{1-\alpha}\right]\\ &+ \frac{1}{(1-\alpha)\Gamma(1-\alpha)}\sum_{j=0}^{k}\left[(j+1)^{1-\alpha}-(j)^{1-\alpha}\right]\sigma(\Delta t^{2-\alpha}).\end{aligned} \tag{2.5}$$

Therefore, the discrete expression for the fractional derivative of Caputo becomes:

ecua11 (2.6)
$$\frac{\partial^{\alpha}u(\mathbf{x},t_{k+1})}{\partial t^{\alpha}} = O\left(\alpha,\Delta t\right)\sum_{j=0}^{k}\left(u\left(\mathbf{x},t_{k-j+1}\right)-u\left(\mathbf{x},t_{k-j}\right)\right)\left[(j+1)^{1-\alpha}-(j)^{1-\alpha}\right]+\sigma(\Delta t^{2-\alpha})$$

By considering the following parameter:

$$O(\alpha,\Delta t)=\frac{1}{\Gamma(1-\alpha)(1-\alpha)\Delta t^{\alpha}}.$$

and the coefficient given by:

$$\omega_j^{(\alpha)}=(j+1)^{1-\alpha}-(j)^{1-\alpha},\quad \forall\, j=0,1,2\cdots,k,$$

the expression in (2.6) is expressed as:

ecua12 (2.7)
$$\frac{\partial^{\alpha}u(x,t_{k+1})}{\partial t^{\alpha}} = O\left(\alpha,\Delta t\right)\sum_{j=0}^{k}\left(u\left(\mathbf{x},t_{k-j+1}\right)-u\left(\mathbf{x},t_{k-j}\right)\right)\omega_j^{(\alpha)}+\sigma(\Delta t^{2-\alpha})$$

If $u_k\left(\mathbf{x}\right)\cong u\left(\mathbf{x},t_k\right)$ represents the approximation of $u\left(\mathbf{x},t_k\right)$, then running the sum to $(j=0)$ then we can rewrite the equation (2.7)

ecua13 (2.8)
$${}_0^cD_t^{\alpha}u(\mathbf{x},t_{k+1})\simeq O\left(\alpha,\Delta t\right)\left(u_{i,j}^{k+1}-u_{i,j}^{k}\right)+O\left(\alpha,\Delta t\right)\sum_{j=1}^{k}\left(u_{i,j}^{k-j+1}-u_{i,j}^{k-j}\right)$$

Discretization for the Spatial Variables. MD methods are characterized by constructing discrete analogs of the classic divergence and gradient operators, in such a way that they satisfy a discrete version of the extended Gauss divergence theorem [9] [1].

Higher-dimensional MD operators can be systematically obtained from their 1D versions using the Kronecker tensor product denoted by $(\otimes)$ and given in [9].

Following the steps of [9], the Cartesian staggered mesh is constructed in 2D (for an example, see Figure 1), so the mimetic discrete analog for the gradient and divergence operators in both X,Y-axes for $\Omega=[a_1,b_1]\times[a_2,b_2]$ are described by:

- m_1 : the number of cells along the X-axis with step size $h_1=(b_1-a_1)/m_1$
- m_2 : the number of cells along the Y-axis with step size $h_2=(b_2-a_2)/m_2$
- Construction of the mimetic mesh on the X and Y axes:

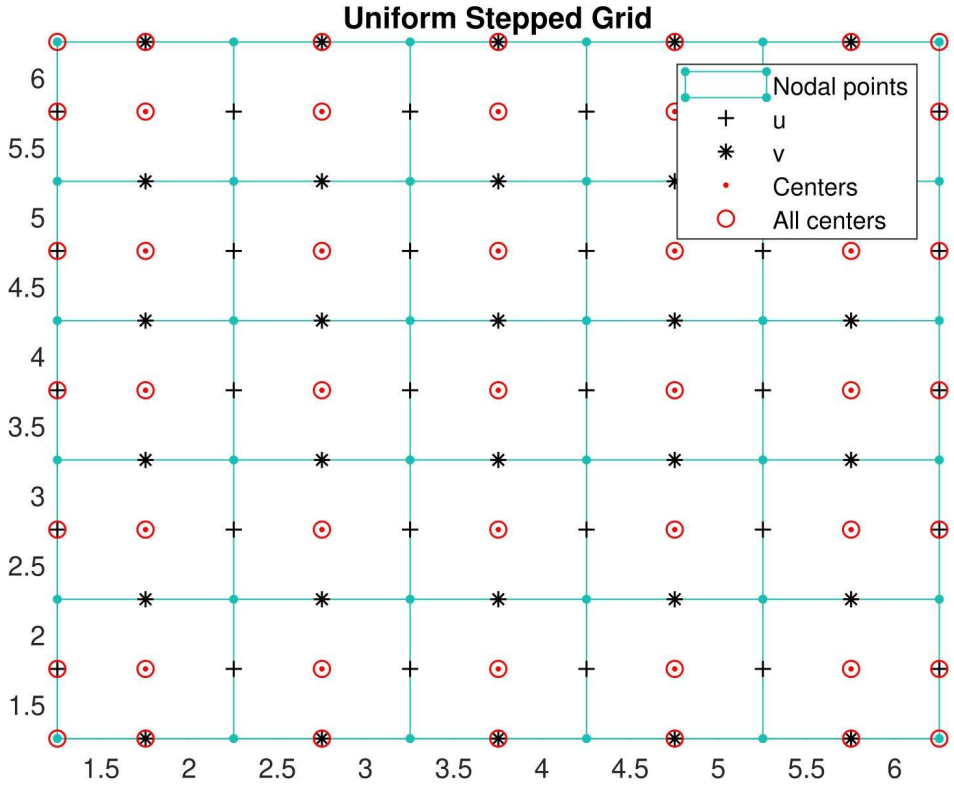

FIGURE 1. Example of a uniform 2D staggered mesh on $[1,6] \times [1,6]$ with five horizontal cells and five vertical cells (each square cell has sides of length one).

- Mesh construction on the X axis:

$$X \quad = \quad \{x_j = a_1 + j(h_1/2);\ j = 0, 1, 2, \cdots, 2m_1\}$$

- Location of the nodes on the X axis:

$$N_1 \quad = \quad \{x_j = a_i + jh_1;\ j = 0, 1, 2, \cdots, m_1\}$$

- Location of the centers on the X axis:

$$C_1 \quad = \quad \{x_j = a_1 + (2j-1)h_1/2;\ j = 1, 2, 3, \cdots, m\}$$

- Formation of centers and border points:

$$S_1 = C_1 \cup \{0, 1\}$$

  The mesh for Y is constructed in the same way.
- The 2D mesh will be expressed as:

$$X \times Y$$

- The centers and borders throughout the 2D grid

$$S = S_1 \times S_2$$

- Location of Nodes on any discrete 2D mesh

$$N = (N_1 \times S_2) \cup (S_1 \times N_2)$$

Then, mimetic operators of divergence and gradient are defined as matrices belonging to the space of all linear transformations, that is:

$$D : N \to S, \qquad G : S \to N$$

2.1. **2D Mimetic Divergence and Gradient Operators.** These operators are defined as:

Given the Cartesian grid S in $[a_1, b_1] \times [a_2, b_2]$, with the number of cells m_1, m_2 on the X and Y axis, respectively, the mimetic operators of the gradient and divergence are constructed, using the Kronecker products.

The 2D divergence operator of order K given in [9], is defined and denoted by:

ecua14 (2.9) $$D_{xy}^{(K)} = \left[D_{xy,2}^{(K)}\right] = \left[\widehat{I}_{m_1} \otimes D_x^{(K)}, D_y^{(K)} \otimes \widehat{I}_{m_2}\right]$$

where $D_x^{(K)}$ is the 1D divergence operator on the X axis given in [1], such that:

$$\widehat{I}_q = \begin{bmatrix} 0_{1\times q} \\ I_{q\times q} \\ 0_{1\times q} \end{bmatrix},$$

where $I_{q\times q}$ is the identity matrix of order $q \times q$.

Furthermore, $D_x 1 = 0$ holds.

Similarly, the 2D gradient operator of order K given in [9] is constructed, defined by:

ecua15 (2.10) $$G_{xy}^{(K)} = \begin{bmatrix} G_{xy,1}^{(K)} \\ G_{xy,2}^{(K)} \end{bmatrix} = \begin{bmatrix} \widehat{I}_n^T \otimes G_x^{(K)} \\ G_y^{(k)} \otimes \widehat{I}_m^T \end{bmatrix}$$

where $G_x^{(K)}$is the 1D gradient operator, on the given X axis in [1] such that:

$$\widehat{I}_q = \begin{bmatrix} 0_{1\times q} \\ I_{q\times q} \\ 0_{1\times q} \end{bmatrix}$$

In addition, it holds $G_{xy} 1 = \vec{0}$.

2.2. **The Boundary Operator.** Mimetic methods are based on the discretization of the classic operators of PDEs such as divergence, gradient, and curl in such a way that they satisfy a discrete version of the divergence theorem utilizing Green's identities [1]

ecua16 (2.11) $$\langle D_d v, f\rangle_Q + \langle v, G_d f\rangle_P = \langle B_d v, f\rangle_I$$

where D_d, G_d represent the discrete analogs of the corresponding continuous gradient (∇) and divergence ($\nabla\cdot$) operators, respectively. I the identity matrix. In addition, d represents the spatial dimension and the functional $\langle\cdot,\cdot\rangle_A$ represents an inner product of the form $\langle v, f\rangle_A \equiv v^T A f$, with weights $A = Q, P$ in (2.11). The boundary operator B_d is defined in [9] by

ecua17 (2.12) $$B_d = Q D_d + (G_d)^T P.$$

2.3. **The Laplace operator.** For a Cartesian grid with m_1 and m_2 cells on the X and Y axes respectively, the discrete 2D Laplace operator of [9] is defined as the product of the corresponding discrete 2D divergence and 2D gradient operators.

Therefore:

$$\begin{aligned} L_x^{(K)} &= D_x^{(K)} \cdot G_x^{(K)} \\ L_{xy}^{(K)} &= D_{xy}^{(K)} \cdot G_{xy}^{(K)} \end{aligned}$$

This mesh contains the coordinates of all functions, both scalar and those defined at the centers of each cell, including the boundary, as well as the coordinates of the vector functions that are defined at each of the nodes of each cell as well as at the boundary of the discrete domain, referenced in the MOLE platform given in [15].

Application of Complete Discretization. From the discretization of the mimetic operators of the gradient and divergence on a uniform stepped mesh of 2D space and the fractional derivative in the Caputo sense discretized by the forward finite difference scheme, the mimetic approximation for the nonlinear Perona-Malik diffusion equation is deduced, which is obtained by substituting the given equations into (2.8), (2.9) and (2.10) in (2.11):

ecua18 (2.13)
$$O(\alpha, \Delta t)\left(u_{i,j}^{k+1} - u_{i,j}^{k}\right) + O(\alpha, \Delta t)\sum_{j=1}^{k}\left(u_{i,j}^{k-j+1} - u_{i,j}^{k-j}\right) = D_{xy}^{(K)}\left(C.G_{xy}^{(K)}\right)u^k$$

Then, the discretization of the Neumann-type boundary is obtained by substituting the (2.12) into (1.2), getting:

ecua19 (2.14)
$$\left(B_{xy}^{(K)}.G_{xy}^{(K)}\right)u^{k+1} = 0$$

From (2.13) and (2.14), we have:

(2.15)
$$\left[O(\alpha, \Delta t) + \left(B_{xy}^{K} \cdot G_{xy}^{K}\right)\right]u^{k+1} = \left[O(\alpha, \Delta t) + D_{xy}^{K}\left(C.G_{xy}^{K}\right)\right]u^k - O(\alpha, \Delta t)\sum_{j=1}^{k}\left(u^{k-j+1} - u^{k-j}\right)$$

The Neumann boundary condition imposed in (1.2), for the case of image processing, indicates a particular way of handling image edges during operations such as filtering or convolution. That is, when we apply a filter or an operation involving a neighborhood to obtain a specific value for the pixel in question, a simple average of neighboring pixels is considered. However, it is important to know what will happen to pixels located at the edge of the image where there are not enough neighbors around the pixel in question to apply the smoothing operation normally.

Therefore, we consider an original image of 862×862 pixels. We can then resize the image to a standard size of 512×512. However, since the Neumann boundary condition is null, the size of the original image can be increased by adding a row and a column to the initial image domain, resulting in a blur, smooth around the image with a dimension of 514×514 [6].

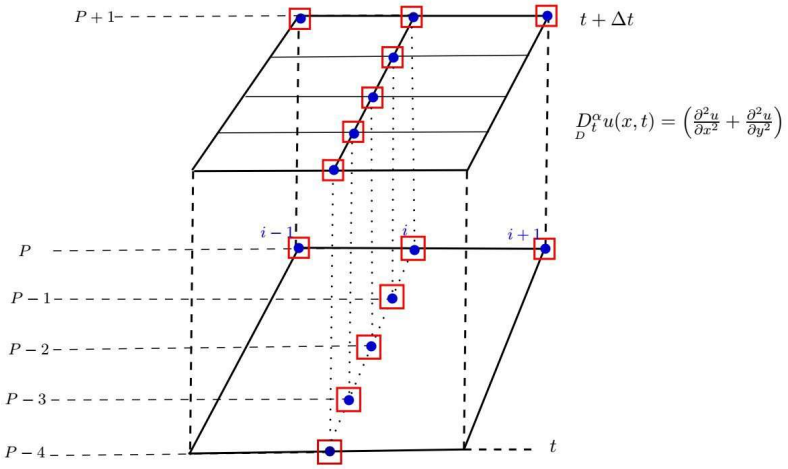

FIGURE 2. Computational Molecule.

Graphical representation of the computational molecule can be found in Figure 2, and it is used to discretize both the spatial and temporal variables.

Any initial color image will always be represented as an 8-bit grayscale ($uint8$) image (black and white), in which each pixel in the image takes an integer value between 0 and 255. Pixel values close to zero (0) become black, pixel values close to one (1) become white, and intermediate values become gray. However, most of the operations in the MATLAB toolbox for diffusion through filtering, convolution, or transforms do not accept integer values and are therefore converted to double values (where pixel values accept decimal numbers, thus providing greater precision in the results).

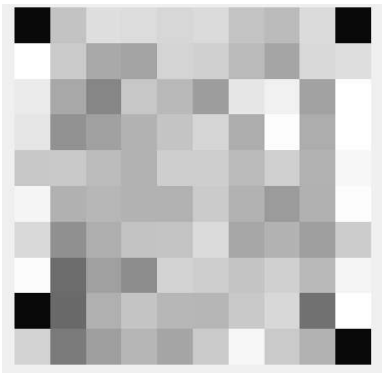

FIGURE 3. Converting a color image to grayscale

The Matlab toolbox is used to employ the commands and functions that allow converting a color image to a black and white image, and then cropping it to a suitable size.

Results and Discussion of the Numerical Simulation. In this section, we present some experimental results obtained from applying the proposed numerical scheme to the original images: Boat, Eye, Mora, and Lena, which have been affected by Gaussian noise. This type of noise is common in images captured with cameras and telescopes that distort all the pixels of the image in question.

(A) Boat (B) Eye (C) Model1 (D) Model2

fig:ab

FIGURE 4. Representation of the original images.

Our proposed model is compared with the results of the standard Perona-Malik model of integer and fractional order using finite differences given in SAMNGO.

Image reconstruction algorithms were implemented in MATLAB-R2018a software, using quantitative metrics to evaluate the performance of our proposed model and quantify the quality of the results obtained from the different methods using PSNR, SNR, and MSE (mean squared error) defined by:

$$\begin{aligned} PSNR &= 10 * \log_{10}\left(\frac{255^2}{\Sigma_{i,j}\left(\widehat{u}-u\right)^2}\right) \\ SNR &= 10 * \log_{10}\left(\frac{\Sigma_{i,j}u^2}{\Sigma_{i,j}\left(\widehat{u}-u\right)^2}\right) \\ MSE &= \frac{1}{MN}\left(\Sigma_{i,j}\left(\widehat{u}-u\right)^2\right) \end{aligned}$$

where u is the original image, $\widehat{u}$ is the restored image, M, N represent the width and height of the image and (i, j) denotes the position of an image element. Then, we compare our results with those shown by [11].

Analysis of the first image. Now we will evaluate the behavior of the noisy images and finally compare them with the original image.

(A) OI (B) FD (C) MFD

FIGURE 5. Evaluation and restoration of the image with Gaussian noise, zero mean, $\sigma = 0.01$ variance and fractional exponent $\alpha = 0.83$. The image on the left corresponds to the original image (OI), the one in the center was obtained using the finite difference (FD) method and the one on the right using the mimetic differences (MD) scheme.

fig:5a

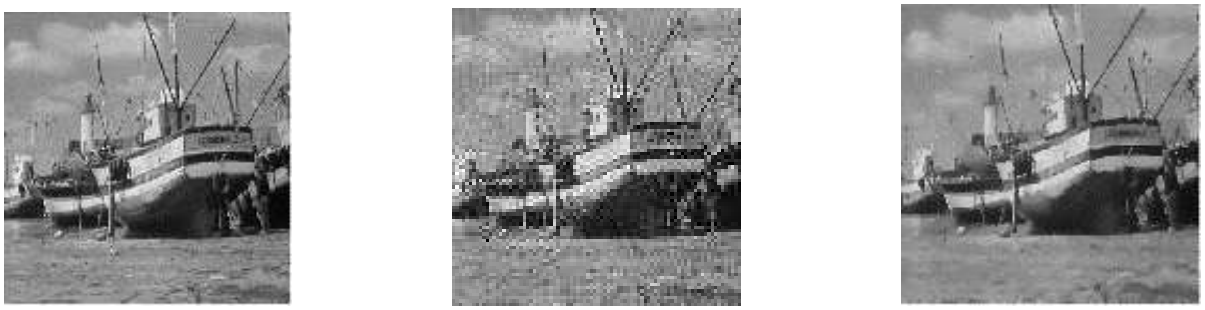

(A) OI (B) FD (C) MFD

FIGURE 6. Evaluation and restoration of the image with Gaussian noise, zero mean, $\sigma = 0.02$ variance and fractional exponent $\alpha = 0.83$. The image on the left corresponds to the original image (OI), the one in the center was obtained using the finite difference (FD) method and the one on the right using the mimetic differences (MD) scheme.

fig:6a

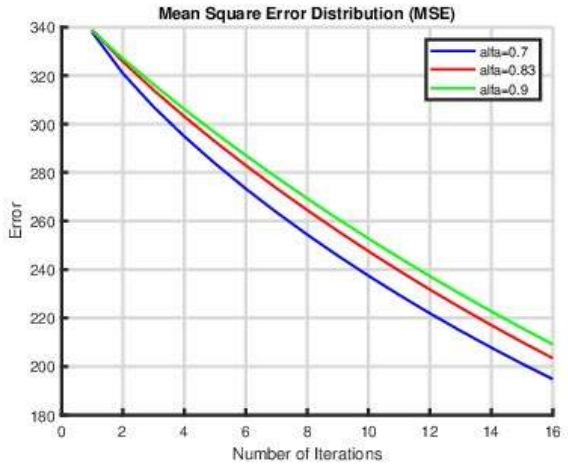

(A) Behavior of the mean squared error for different values of alpha.

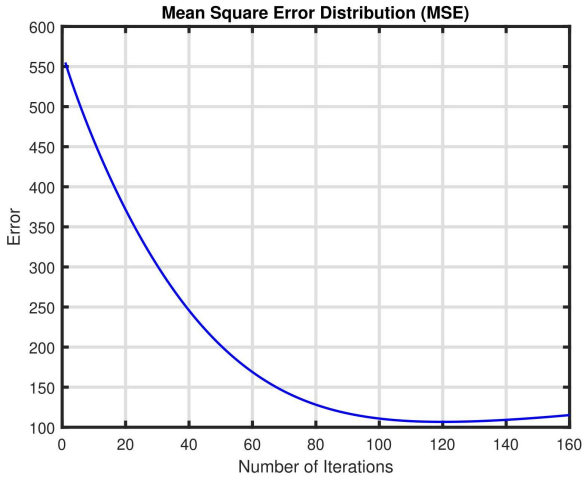

(B) Mean squared error behavior for a given alpha value.

FIGURE 7. The figure shown in part (a) indicates how the mean squared error moves with respect to the number of iterations for the values of $\alpha = 0.7$, $\alpha = 0.83$, and $\alpha = 0.9$, while the figure on the right hand (b) indicates the proximity, of the restored image to the original image which indicates that the best approximation is achieved at iteration 120

fig:7a

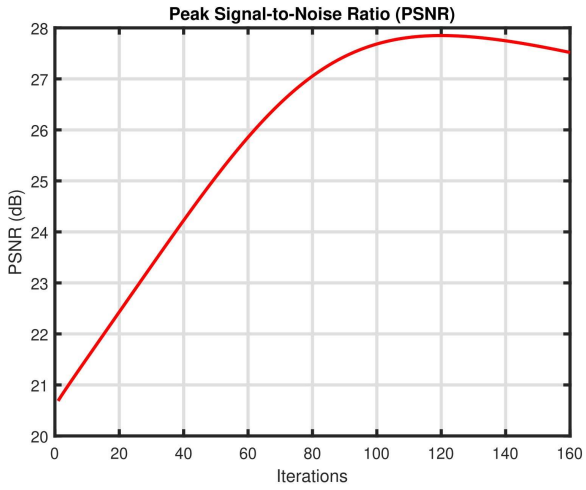

(A) Metric that indicates the improvement of the restored image

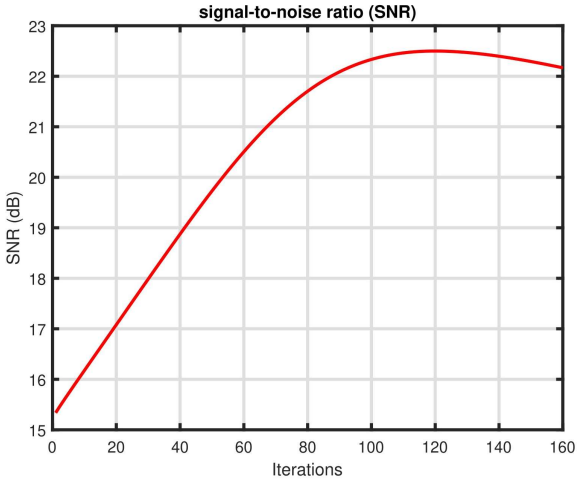

(B) Metric that indicates the improvement of the restored image

FIGURE 8. PSNR and SNR are metrics that are calculated at each step of the iteration to evaluate the improvement of the noisy image.

fig:8a

METRICS THAT INDICATE THE IMPROVEMENT OF THE RESTORED IMAGE				
MODEL	NUMERICAL TECHNIQUES	S.N.R	P.S.N.R	M.S.E
Boat N× M = 510 × 510 k = 6 $\Delta t = 0.1$ $\Delta x = 1$ $\Delta y = 1$ Mean = 0	Finite Difference Method Perona-Malik of Integer Order $\sigma = 0.01$	17.9907	24.1097	
	Finite Difference Method Perona-Malik of Factional Order $\sigma = 0.01$, $\alpha = 0.83$	21.3823	27.4801	
	Mimetic Differences Method Perona-Malik of fractional Order $\sigma = 0.01$, $\alpha = 0.83$	24.7252	30.0759	65.8362
	Finite Difference Method Perona-Malik of Fractional Order $\sigma = 0.01$, $\alpha = 0.9$	20.8720	27.0342	
	Mimetic Differences Perona-Malik of Fractional Order $\sigma = 0.01$, $\alpha = 0.9$	24.6599	30.0105	65.4420

TABLE 1. Efficiency of the Proposed Method in Image Recovery with Gaussian Variance ($\sigma = 0.01$)

Table 1 shows that the results obtained using the mimetic differences technique for restoring images of the fractional-time Perona-Malik model from a Gaussian noise image with zero mean, variance ($\sigma = 0.01$), and fractional exponent ($\alpha = 0.83$) indicate a better result compared to the results presented by [11]. Furthermore, the highest SNR value is 24.7252, which is much higher than that reported in [11]. Similarly, the best PSNR value is 30.759, exceeding the PSNR value reported in the aforementioned article. Similarly, it is observed that when considering a new value of the fractional exponent ($\alpha = 0.9$), the best SNR and PSNR values are reached at 24.6599 and 30.0105, and again, despite a slight decrease with the previous value of the fractional exponent, it is verified that the numerical technique proposed in this work improves the results shown in [11].

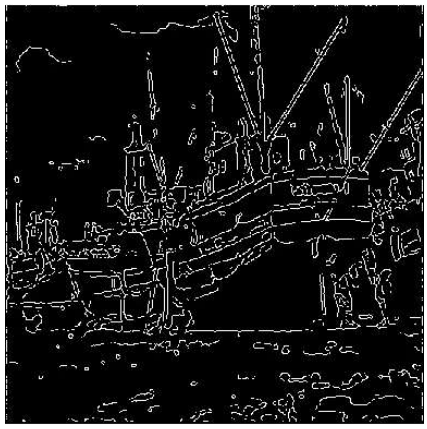

(A) Edge Presentation

fig:9a

FIGURE 9. Edge detection using the Canny algorithm

Analysis of the second image. Now we will evaluate the behavior of the second image.

(A) OI (B) FD (C) MD

FIGURE 10. Evaluation and restoration of the image with Gaussian noise, zero mean, $\sigma = 0.01$ variance and fractional exponent $\alpha = 0.63$. The image on the left corresponds to the original image (OI), the one in the center was obtained using the finite difference (FD) method and the one on the right using the mimetic differences (MD) scheme.

fig:5

(A) OI (B) FD (C) MD

FIGURE 11. Evaluation and restoration of the image with Gaussian noise, zero mean, $\sigma = 0.02$ variance and fractional exponent $\alpha = 0.63$. The image on the left corresponds to the original image (OI), the one in the center was obtained using the finite difference (FD) method and the one on the right using the mimetic differences (MD) scheme.

fig:6

(A) Behavior of the mean squared error for different values of alpha.

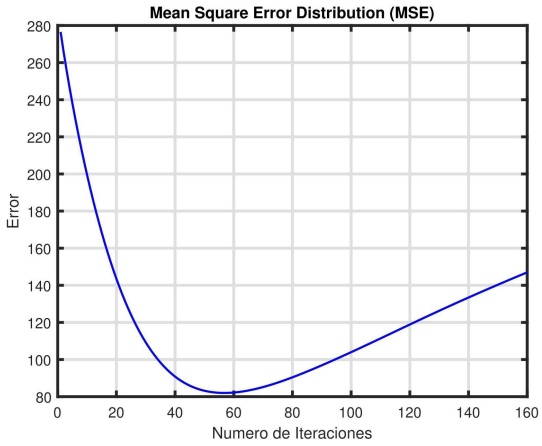

(B) Mean squared error behavior for a given alpha value.

FIGURE 12. The figure shown in part (a) indicates how the mean squared error moves with respect to the number of iterations for the values of $\alpha = 0.63$, $\alpha = 0.83$, and $\alpha = 0.9$. The figure (b) indicates the proximity, of the restored image to the original image which indicates that the best approximation is achieved at iteration 57

fig:7

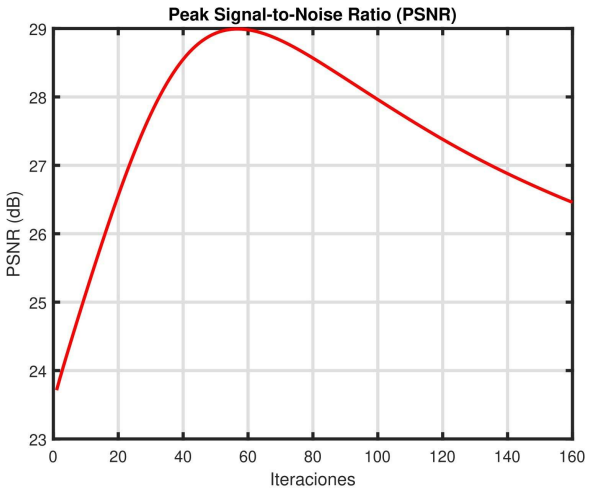

(A) Metric that indicates the improvement of the restored image

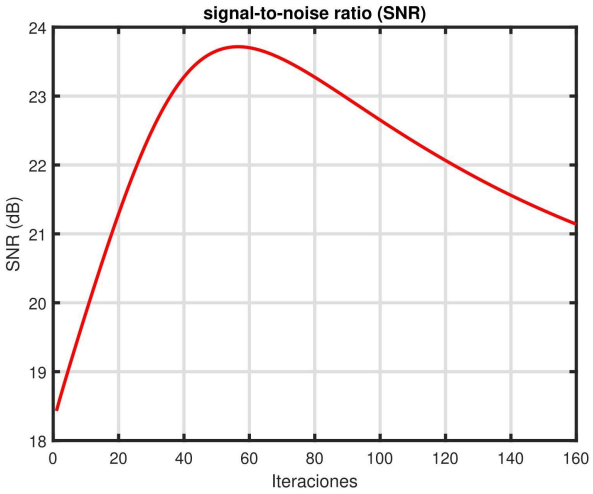

(B) Metric that indicates the improvement of the restored image

FIGURE 13. It is important to note that the SNR and PSNR metrics used to measure the quality of image restoration indicate that the best image is obtained approximately after the 57 iteration and that they should result in the best image quality, that is, the image becomes sharper and loses noise or is also called a blurry image.

fig:8

METRICS THAT INDICATE THE IMPROVEMENT OF THE RESTORED IMAGE				
MODEL	NUMERICAL TECHNIQUES	S.N.R	P.S.N.R	M.S.E
Eye $N \times M = 450 \times 450$ $k = 6$ $\Delta t = 0.1$ $\Delta x = 1$ $\Delta y = 1$ Mean = 0	Finite Difference Method Perona-Malik of Integer Order $\sigma = 0.01$	18.3240	23.5775	
	Finite Difference Method Perona-Malik of Factional Order $\sigma = 0.01$, $\alpha = 0.63$	20.9576	26.2677	
	Mimetic Differences Method Perona-Malik of fractional Order $\sigma = 0.01$, $\alpha = 0.63$	23.7144	29.0326	112.3390
	Finite Difference Method Perona-Malik of Fractional Order $\sigma = 0.01$, $\alpha = 0.81$	21.0049	26.8741	
	Mimetic Differences Perona-Malik of Fractional Order $\sigma = 0.01$, $\alpha = 0.81$	23.7372	29.0554	90.5801

TABLE 2. Efficiency of the Proposed Method in Image Recovery with Gaussian Variance ($\sigma = 0.01$)

Table 2 shows that the results obtained using the mimetic differences technique for restoring images of the fractional-time Perona-Malik model from a Gaussian noise image with zero mean, variance ($\sigma = 0.01$), and fractional exponent ($\alpha = 0.63$) indicate a better result compared to the results presented by [11]. Furthermore, the highest SNR value is 23.7144, which is much higher than that reported in [11]. Similarly, the best PSNR value is 29.0326, exceeding the PSNR value reported in the aforementioned article. Similarly, it is observed that when considering a new value of the fractional exponent ($\alpha = 0.81$), the best SNR and PSNR values are reached at 23.7372 and 29.0554, and again, despite a slight decrease with the previous value of the fractional exponent, it is verified that the numerical technique proposed in this work improves the results shown in [11].

(A) Edge Presentation

fig:9

FIGURE 14. Edge detection using the Canny Algorithm

Analysis of the third image. Now we will evaluate the behavior of the third image.

(A) OI (B) FD (C) MD

FIGURE 15. Evaluation and restoration of the image with Gaussian noise, zero mean, $\sigma = 0.01$ variance and fractional exponent $\alpha = 0.7$. The image on the left corresponds to the original image (OI), the one in the center was obtained using the finite difference (FD) method and the one on the right using the mimetic differences (MD) scheme.

fig:5b

(A) OI (B) FD (C) MD

FIGURE 16. Evaluation and restoration of the image with Gaussian noise, zero mean, $\sigma = 0.02$ variance and fractional exponent $\alpha = 0.7$. The image on the left corresponds to the original image (OI), the one in the center was obtained using the finite difference (FD) method and the one on the right using the mimetic differences (MD) scheme.

fig:6b

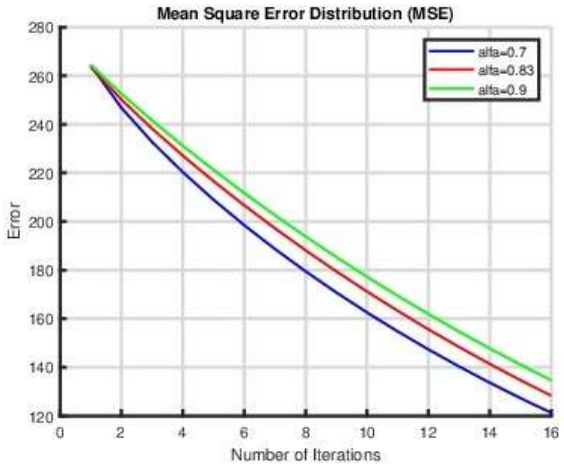

(A) Behavior of the mean squared error for different values of alpha

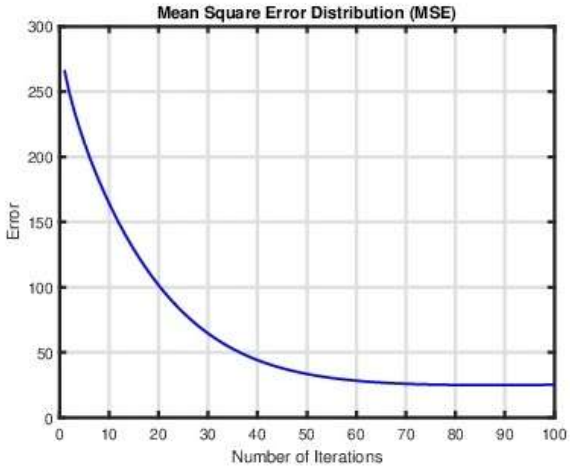

(B) Mean squared error behavior for a given alpha value

FIGURE 17. The figure shown in part (a) indicates how the mean squared error moves with respect to the number of iterations for the values of $\alpha = 0.7$, $\alpha = 0.83$, and $\alpha = 0.9$. The figure (b) indicates the proximity, of the restored image to the original image which indicates that the best approximation is achieved at iteration 85.

fig:7b

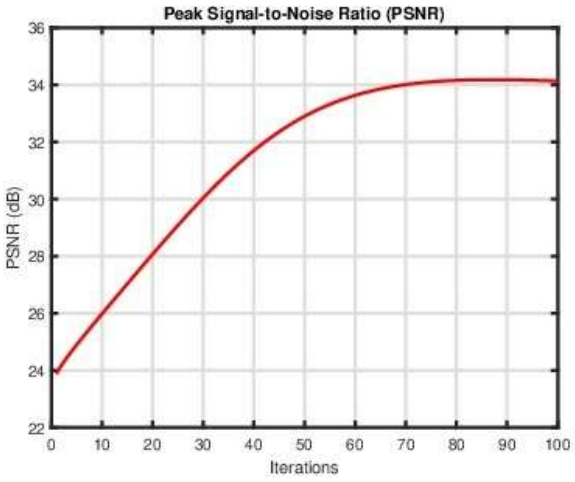

(A) Metric that indicates the improvement of the restored image.

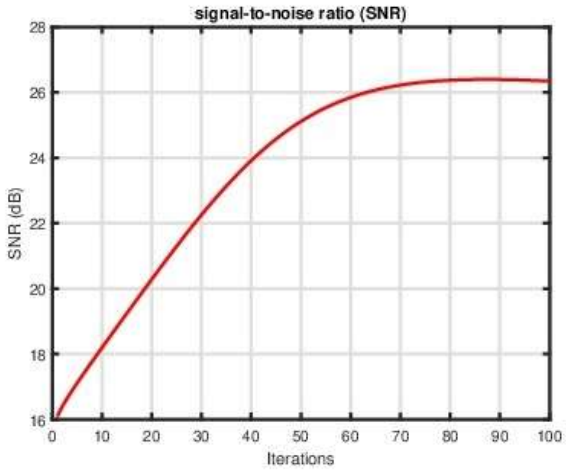

(B) Metric that indicates the improvement of the restored image

FIGURE 18. It is important to note that the SNR and PSNR metrics, used to measure the quality of image restoration, indicate that the best image is obtained approximately after iteration 85 and that a better image quality should result; that is, the image becomes sharper and loses noise, or in other words, a blurry image.

fig:8b

METRICS THAT INDICATE THE IMPROVEMENT OF THE RESTORED IMAGE				
MODEL	NUMERICAL TECHNIQUES	S.N.R	P.S.N.R	M.S.E
Model1 $N \times M = 509 \times 509$ $k = 6$ $\Delta t = 0.1$ $\Delta x = 1$ $\Delta y = 1$ Mean = 0	Finite Difference Method Perona-Malik of Integer Order $\sigma = 0.01$	19.4911	24.8358	
	Finite Difference Method Perona-Malik of Factional Order $\sigma = 0.01$, $\alpha = 0.7$	22.1066	27.4772	
	Mimetic Differences Method Perona-Malik of fractional Order $\sigma = 0.01$, $\alpha = 0.7$	26.3938	34.1757	25.1562
	Mimetic Differences Method Perona-Malik of Fractional Order $\sigma = 0.02$, $\alpha = 0.7$	23.5929	31.3747	47.3946

TABLE 3. Efficiency of the proposed numerical method in the recovery of images with zero mean, Gaussian noise and variances ($\sigma = 0.01, 0.02$)

Table 3 shows that the results obtained using the mimetic differences technique for restoring images of the fractional-time Perona-Malik model from a Gaussian noise image with zero mean, variance ($\sigma = 0.01$), and fractional exponent ($\alpha = 0.7$) indicate a better result compared to the results presented by [11]. Furthermore, the highest SNR value is 26.3938, which is much higher than that reported in [11]. Similarly, the best PSNR value is 34.1757, exceeding the PSNR value reported in the aforementioned article. Similarly, it is observed that when considering a new variance ($\sigma = 0.02$), the best SNR and PSNR values are achieved at 23.5929 and 31.3747, respectively. Again, despite a slight decrease compared to the previous value of the fractional exponent, it is verified that the numerical technique proposed in this work improves the results shown in [11].

(A) Edge Presentation

fig:9b

FIGURE 19. Edge detection using the Canny Algorithm

Analysis of the fourth image. Now we will evaluate the behavior of the fourth image.

(A) OI (B) FD (C) MD

FIGURE 20. Evaluation and restoration of the image with Gaussian noise, zero mean, $\sigma = 0.01$ variance and fractional exponent $\alpha = 0.7$. The image on the left corresponds to the original image (OI), the one in the center was obtained using the finite difference (FD) method and the one on the right using the mimetic differences (MD) scheme.

fig:5c

(A) OI (B) FD (C) MD

FIGURE 21. Evaluation and restoration of the image with Gaussian noise, zero mean, $\sigma = 0.02$ variance and fractional exponent $\alpha = 0.7$. The image on the left corresponds to the original image (OI), the one in the center was obtained using the finite difference (FD) method and the one on the right using the mimetic differences (MD) scheme.

fig:6c

The data obtained from the matrices used to locate the sharpest and cleanest image, free of noise, will then be discussed. When the mean squared error (MSE) approaches zero, the maximum signal-to-noise ratio (PSNR) increases considerably, and this implies that a high PSNR indicates the best image quality.

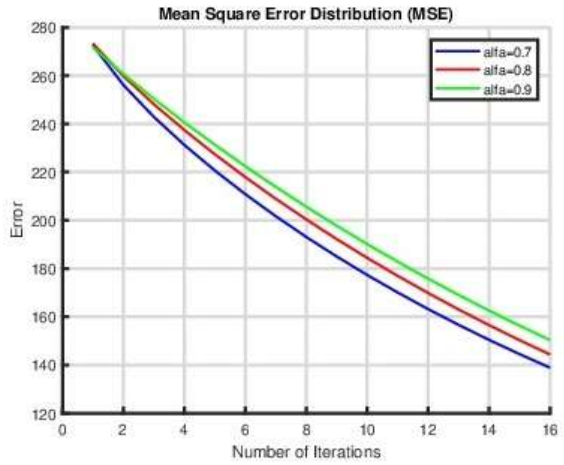

(A) Behavior of the mean squared error for different values of alpha.

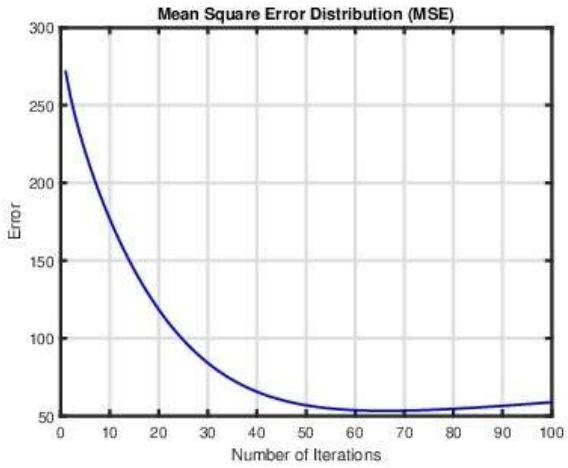

(B) Mean squared error behavior for a given alpha value.

FIGURE 22. The figure shown in part (a) indicates how the mean squared error moves with respect to the number of iterations for the values of $\alpha = 0.7$, $\alpha = 0.8$, and $\alpha = 0.9$. The figure (b) indicates the proximity, of the restored image to the original image which indicates that the best approximation is achieved at iteration 67

fig:7c

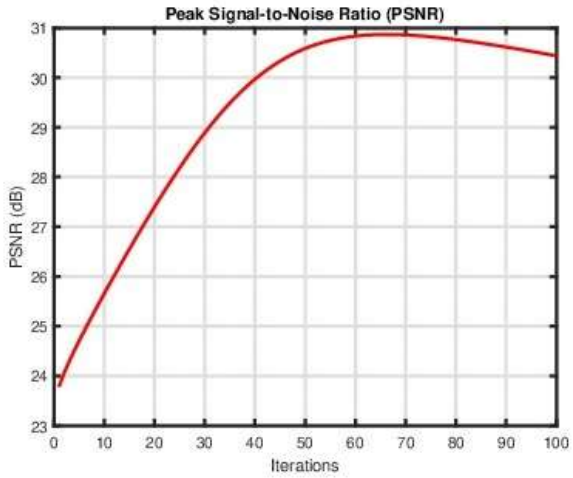

(A) Metric that indicates the improvement of the restored image.

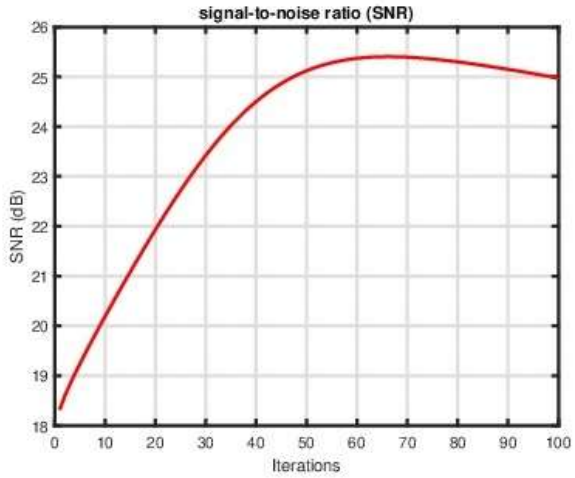

(B) Metric that indicates the improvement of the restored image

FIGURE 23. It is important to note that the SNR and PSNR metrics used to measure the quality of image restoration indicate that the best image is obtained approximately after the 67 iteration and that they should result in the best image quality, that is, the image becomes sharper and loses noise or is also called a blurry image.

fig:8b0

METRICS THAT INDICATE THE IMPROVEMENT OF THE RESTORED IMAGE				
MODEL	NUMERICAL TECHNIQUES	S.N.R	P.S.N.R	M.S.E
Lena $N \times M = 507 \times 507$ $k = 6$ $\Delta t = 0.1$ $\Delta x = 1$ $\Delta y = 1$ Mean = 0	Finite Difference Method Perona - Malik of Integer Order $\sigma = 0.02$	15.7359	21.3160	
	Finite Difference Method Perona - Malik of Factional Order $\sigma = 0.02$, $\alpha = 0.8$	19.9973	24.9802	
	Mimetic Differences Method Perona - Malik of fractional Order $\sigma = 0.02$, $\alpha = 0.8$	23.2436	28.7085	99.8792
	Finite Difference Method Perona - Malik of Fractional Order $\sigma = 0.02$, $\alpha = 0.9$	19.0326	24.6910	
	Mimetic Differences Perona - Malik of Fractional Order $\sigma = 0.02$, $\alpha = 0.9$	23.2230	28.6879	100.7839

TABLE 4. Efficiency of the proposed numerical method for image recovery with Gaussian noise and variance($\sigma = 0.02$)

Tabla 4 shows that the results obtained using the mimetic differences technique for restoring fractional-time Perona-Malik model images from a Gaussian noise image with zero mean, variance ($\sigma = 0.02$), and fractional exponent ($\alpha = 0.8$) show a better result compared to the results presented by [11]. Furthermore, the highest SNR value is 23.2436, significantly higher than that reported by [11]. Similarly, the best PSNR value is 28.7085, exceeding the PSNR value reported in the aforementioned article.

Similarly, it is observed that when considering a new value for the fractional exponent ($\alpha = 0.9$), the best SNR and PSNR values are achieved at 23.2230 and 28.6879, respectively. Again, despite a slight decrease compared to the previous value of the fractional exponent, it is verified that the numerical technique proposed in this work improves the results shown in [11].

(A) Edge

FIGURE 24. Edge detection using the Canny Algorithm

In Figure 24 we present the results of edge detection with the Canny algorithm.

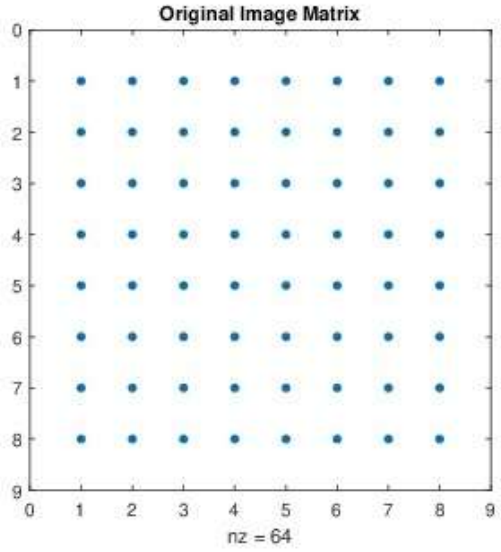

FIGURE 25. Matrix Representation of the Original Image.

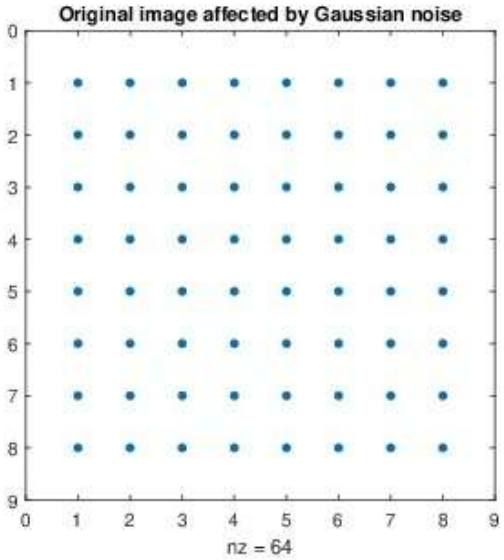

FIGURE 26. Matrix Representation of the Image Affected by Gaussian Noise.

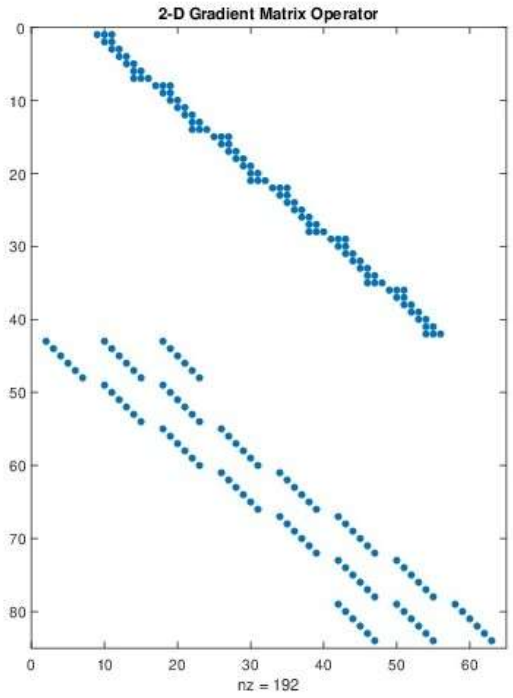

FIGURE 27. Matrix Representation of the 2D Gradient.

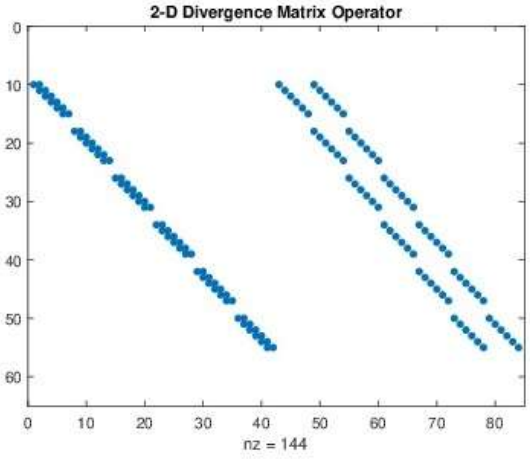

FIGURE 28. Matrix Representation of 2D Divergence.

Figures 25 and 26 show the transformation of an original image into its matrix form using the Matlab toolbox applications, while Figures 27 and 28 represent the matrix form of the discrete gradient and divergence operators.

Below we detail the code described in Matlab version R2018a for the simulation in image processing of the Perona-Malik model of fractional order in time, by combining the numerical scheme of mimetic differences in [9] and the explicit finite difference scheme.

3. Matlab code for the Perona-Malik Fractional Time-Order Nonlinear Anisotropic Model

```
1
2  clc; clear; close all
3
4  addpath('./mole_MATLAB')
5
6  Read lena image
7
8  n = 400;
9
10 num_iter = 160;
11 alpha_f = 0.9;
12
13 RGB = imread('Boat_(test_image).jpg');
14
15 m=size(RGB,1);
16 n=m;
17 a=0;
18 b=m;
19 c=0;
20 d=m;
21 dx=(b-a)/m;
22 dy=(d-c)/m;
23
24 RGB = padarray(RGB,[1  1],255,'both');
25 RGB(1,:) = RGB(2,:);
26 RGB(end  ,:)= RGB(end-1  ,:);
27 RGB(:,1)= RGB(:,2);
28 RGB(:,end)= RGB(:,end-1);
29
30
31 I = rgb2gray(RGB);
32 I0X = imnoise(RGB, 'gaussian',0,0.01);
33
34 I0X = rgb2gray(I0X);
35
36 I_original = double(I)+1;
37
38 IX  = double(I0X)+1;
39 k = 2;
40
41 % 2D Staggered grid
42 xgrid = [a a+dx/2 : dx : b-dx/2 b];
43 ygrid = [c c+dy/2 : dy : d-dy/2 d];
44
45 % 2D Mimetic Divergence Gradient Operators
46 D = div2D(k, m, dx, n, dy);
47 G = grad2D(k, m, dx, n, dy);
48
49 alpha =1;
50
51 dt = 0.1;
52
53 % Initial Condition Image
54 I2 = IX;
```

```
55
56 k_f = 6;
57 w = zeros((n+2)^2,num_iter);
58 mse_values = zeros(num_iter,1);
59 snr = zeros(num_iter,1);
60 psnr_values = zeros(num_iter,1);
61
62 sigma = (gamma(2-alpha_f)*(dt^alpha_f));
63
64 %IMMSE..... 1
65
66
67 I2  = reshape(I2, [], 1);
68 w(:,1) = I2;
69 I3 = G*w(:,1);
70
71 C = 1./(1+(I3./k_f).^2);
72 L1 = C.*I3;
73 w(:,2) = w(:,1) + D*L1*sigma;
74
75
76 mse_values(1) = immse(reshape(w(:,1), n+2, n+2), I_original);
77 psnr_values(1)= 10*log10(255^2/mse_values(1));
78 snr(1) = 10*log10(immse(zeros(n+2,n+2),I_original)/mse_values(1));
79
80 mse_values(2) = immse(reshape(w(:,2), n+2, n+2), I_original);
81 psnr_values(2)= 10*log10(255^2/mse_values(2));
82 snr(2) = 10*log10(immse(zeros(n+2,n+2),I_original)/mse_values(2));
83
84 for t = 2 : num_iter-1
85
86 suma = 0;
87 omega_t = (t+1)^(1-alpha_f) - (t)^(1-alpha_f);
88 for jj=2:t
89 suma = suma + omega_t*(w(:,t-jj+2)-w(:,t-jj+1));
90 end
91
92 I3 = G*w(:,t);
93 C = 1./(1+(I3./k_f).^2);
94 L1 = C.*I3;
95
96
97 w(:,t+1)= D*L1*sigma + w(:,t) - suma;
98
99 mse_values(t+1) = immse(reshape(w(:,t+1), n+2, n+2), I_original);
100 psnr_values(t+1)= 10*log10(255^2/mse_values(t+1));
101 snr(t+1) = 10*log10(immse(zeros(n+2,n+2),I_original)/mse_values(t+1));
102 end
103
104
105 I2=reshape(w(:,num_iter), n+2, n+2);
106 I2=uint8((I2-1));
107
108 [maxsnr,posicion] = max(snr);
109 [maxpsnr_values,posicion1] = max(psnr_values);
110 fprintf('El maximo SNR es %.4f y se alcanza en la iteracion %d\n',maxsnr,
      posicion);
```

```
fprintf('Error cuadratico Medio =%.4f\n',mse_values(end));
fprintf('Se\~nal Ruido Pico =%.4f\n' y se alcanza en la iteracion %d\n',
    maxpsnr_values,posicion1);

figure;
plot(1:num_iter, mse_values, 'b-', 'LineWidth', 1.5);
xlabel('Numero de Iteraciones');
ylabel('Error');
title('Distribucion del Error Cuadr\'atico Medio')
grid on;
figure;
plot(1:num_iter, psnr_values, 'r', 'LineWidth', 2);
xlabel('Iteraciones');
ylabel('PSNR (dB)');
title('Peak Signal-to-Noise Ratio (PSNR)');
grid on;

figure;
plot(1:num_iter, snr, 'r', 'LineWidth', 2);
xlabel('Iteraciones');
ylabel('SNR (dB)');
title(' (SNR)');
grid on;

figure
subplot(1,2,1)
imshow(I)
title('Original Image')
subplot(1,2,2)
imshow(I2)
title('Perona Malik Image')
figure
BW1 = edge(I,'Canny');
BW2 = edge(I2,'Canny');
imshowpair(BW1,BW2,'montage')
```

4. Conclusions

This research paper presents a novel numerical method for solving the fractional-time nonlinear anisotropic Perona-Malik diffusion equation with Neumann boundary conditions on a two-dimensional uniform stepped grid. This numerical method combines mimetic and explicit finite differences. Mimetic differences were used to discretize the spatial variables, and explicit finite differences to discretize the temporal variable. We applied the proposed numerical technique to the fractional-time Perona-Malik model to smooth images to which we added Gaussian noise. We compared the results obtained from the proposed numerical scheme with the classical Perona-Malik model and with the fractional-time Perona-Malik model, both solved numerically using the explicit finite difference scheme. We present the results calculated using the signal-to-noise ratio (SNR) and peak signal-to-noise ratio (PSNR) metrics, observing that the values obtained with these metrics for the proposed model show a significant superiority compared to the other models mentioned.

References

CJYM [1] J. Castillo and M. Yasuda *Linear systems arising for second-order mimetic divergence and gradient discretizations*, Journal of Mathematical Modelling and Algorithms. pp. 67-82, (2005). 6, 8

LYXC [2] Y. Lin and C. Xu *Finite difference/spectral approximations for the time-fractional diffusion equation*, Journal of Computational Physics. pp. 1533-1552, (2007). 5

HSLZCW [3] S. Hu, Z. Liao, and W. Chen,*Sinogram Restoration for Low-Dosed X-Ray Computed Tomography Using Fractional-Order Perona-Malik Diffusion*, Hindawi Publishing Corporation Mathematical Problems in Engineering. pp. 13, (2012). 2

MB [4] B. Maiseli, *Nonlinear anisotropic diffusion methods for image denoising problems: Challenges and future research opportunities*, Array 17 (2023). 2

ASARIAMY [5] S. Abd, R. Abdul, A. Ibrahim and Y. Manurung *Application of Perona Malik Anisotropic Diffusion on Digital Radiographic Image*, Aip Conference Proceedings. pp. 46-51, 2014. 2

PPMJ [6] P. Perona and J. Malik. *Scale space and edge detection using anisotropic diffusion*, IEEE Transactions on Pattern Analysis and Machine Intelligence. 12(7) pp. 629-639, 1990. 4, 5, 9

YJWJ [7] J. Yuan and J. Wang, *Perona-Malik model with a new diffusion coefficient for image denoising*, International Journal of Image and Graphics. vol. 16, 2016. 5

KVRANK [8] V. Kamalaveni, R. Rajalakshmi, and K. Narayanankutty *Image denoising using variations of Perona-Malik model with differents edges stopping functions*, Computer Science, vol. 58, pp. 673-682, 2015. 5

CJCJ [9] J. Corbino and J. Castillo *J. Corbino, J. Castillo, Higher order mimetic finite difference operators satisfying a Gauss Divergence Theorem*, Journal of Computational and Applied Mathematics, 2018. 6, 8, 9, 25

YJYJZS [10] J. Yu, J. Yin, S. Zhou, S. Huang and X. Xie *An image super-resolution reconstruction model based on fractional-order anisotropic difusion equation*, Mathematical Biosciences and Engineering pp.18(5): 6581-6607, (2021). 2

SAMNGO [11] A. Sayah, N. Moussaid, and O. Gouasnouane *Finite difference method for Perona-Malik model with fractional derivative and its application in image processing*, EasyChair Preprint, (2022). 3, 4, 11, 14, 17, 20, 23

NGANNJ [12] G. Nyotoka, N. Ally and J. Nombo *Diffusion-Steered Algorithm for Improving Quality of Images Generated by Electrical Capacitance Tomography Measurement System*, Tanzania Journal of Science pp. 50(2): 387-396, (2024). 3

CJDM [13] J. Carrillo and M. Dumett *Image Shock Filtering With Mimetic Differences*, Computational Science and Engineering Publication Number: CSRCR2024-04, (2024). 3, 4

DJANNJMA [14] J. Dismas, N. Ally, J. Nombo, A. Mwambela, and B. Maiseli *Perona-Malik Diffusion-Driven Regularization for Image Resolution Enhancement in Electrical Capacitance Tomography*, Tanzania Journal of Engineering and Technology: pp. 43(2):139-149, (2024). 3

CJCJM [15] J. Corbino, J. Castillo and Mole *Mimetic Operators Library Enhanced: The Open Source Library for Solving Partial Differential Equations Using Mimetics Methods*, Version v2.0., doi: 10.5281/zenodo.7996615. GitHub, https://github.com/csrc-sdsu/mole, (2023). 3, 4, 9

TAJM [16] A. Tiarimti and M. Jourhmane *Edge-preserving smoothing of Perona-Malik nonlinear diffusion in two-dimensions*, Int. J. Nonlinear Anal Appl. Vol 16, (2025).

SK [17] K. Shi *Image denoising by nonlinear nonlocal diffusion equations*, Journal of Computational and Applied Mathematics. 395 (2021).

LDAFR [18] A. De Luca, R. Folino and M. Strani *Layered Patterns in Reaction-Diffusion Models with Perona-Malik Diffusions*, Milan Journal of Mathematics. Vol 92, pp. 195-234, (2024).

(M. Gonzales Herrera)
Departamento de Matemáticas
Universidad Nacional Pedro Ruiz Gallo
Av. Juan XXIII s/n, Lambayeque, Peru
Email address: mgonzalesh@unprg.edu.pe

(S. Murillo)
Universidad Nacional Trujillo
Av. Juan Pablo II s/n., Trujillo, Peru
Email address: sauloedison.mc@gmail.com

(M. Dumett)
Computational Science Research Center
San Diego State University
5500 Campanile Drive, San Diego, CA 92182, USA
Email address: mdumett@sdsu.edu